FOURTEENTH EUROPEAN ROTORCRAFT FORUM

15

Paper No. 10

EXPERIMENTAL STUDY OF THE FLOW AROUND AN HELICOPTER FUSELAGE. COMPARISON WITH THREE-DIMENSIONAL BOUNDARY LAYER CALCULATIONS.

C. GLEYZES - X. de SAINT-VICTOR
ONERA-CERT, TOULOUSE (FRANCE)
A. CLER
AEROSPATIALE, MARIGNANE (FRANCE)

20-23 September, 1988
MILANO ITALY

ASSOCIAZIONNE INDUSTRIE AEROSPAZIALI
ASSOCIATIONNE ITALIANA DI AERONAUTICA ED ASTRONAUTICA

EXPERIMENTAL STUDY OF THE FLOW AROUND AN HELICOPTER FUSELAGE. COMPARISON WITH THREE-DIMENSIONAL BOUNDARY LAYER CALCULATIONS.

C. GLEYZES - X. de SAINT-VICTOR
ONERA-CERT, TOULOUSE (FRANCE)
A. CLER
AEROSPATIALE, MARIGNANE (FRANCE)

1 Introduction

A better prediction of the aerodynamic characteristics of helicopter fuselages goes through validation of calculation procedures on well documented test cases.

The aim of this study was to provide detailed experimental results on a simplified fuselage model, in order to try to fulfill this requirement. The geometry of this model (designed and provided by AEROSPATIALE) has been chosen (Fig. 1) according to the following criteria :

- analytical representation of the body, so that grid generation would be easy to realize and does not add to the complexity of the problem ;
- important flat surfaces, to make boundary layer LDV measurements possible on a large part of the model ;
- rapid contraction at the junction with the tail boom, in order to induce important separations.

Contribution of ONERA/CERT/DERAT in this program was first the experimental study of this model in the F2 wind tunnel. Another part of this work consisted in three-dimensional boundary layer calculations on this body, aimed on a possible interaction with potential flow calculation procedures developed at ONERA.

2 Experimental set up - Measurements

The model was tested in F2 wind tunnel, which is specially devoted to research programs /Ref. 1/. Its test section (1.4 x 1.8 m^2) is fitted, along 5 m, with interchangeable lateral walls allowing a very flexible use of glass, plexiglass and wood. This characteristic allows access to almost all the test section with three-dimensional LDV system.

This LDV system uses three colors (blue, green and violet) giving in the measuring volume three sets of interference fringes in three different directions. Blue and green beams use a common optical path and provide two orthogonal projections of the velocity vector. The third set of violet beams uses a second path and provides a third projection of the velocity, in a direction as close as possible to the normal to the two previous ones (Fig. 2). Doppler signals are then collected through three photomultipliers and processed by the three frequency counters. The computer stores then on a tape the three frequencies plus the time, only if the three frequency information arrive within a given time window, to ensure significant simultaneity of the signals.

To be able to transform frequencies in velocity vectors, a preliminary step consists, at the beginning of the test period, in measuring the angles of the six individual beams, relative to vertical and horizontal references. These twelve angular measurements provide then, for each color :

- angle between beams and consequently the distance between the fringes,
- direction of the corresponding projection of the velocity vector relative to tunnel references.

The first series of data provide the magnitude of each projection of the velocity. The second series provide the transformation matrix from the coordinate system defined by the three projections, to the tunnel coordinate system. If user provides transformation matrix from tunnel coordinate system to model coordinate system, results are then reduced in this reference system (for instance, a system related to the local normal to the body at a given location for boundary layer measurements).
For processing these data, 2 000 samples are taken, providing 2 000 instantaneous velocity vectors in user coordinate system, and a statistical treatment gives the three components of mean velocity, and the six components of Reynolds stress tensor.

The three-dimensional LDV system has been widely used to provide detailed experimental results in two characteristic configurations :

$$\alpha = 0^o \text{ and } \alpha = -5^o \text{ , for } U_\infty = 40 ms^{-1}$$

Boundary layer surveys at around 40 locations on the model provide useful comparisons with calculation method. Wake surveys in two planes normal to the model axis will give very helpful results for validations of wake modelling methods, but are also of great interest in relation with separation patterns.

Besides these LDV measurements, other techniques were used :

- Oil flow visualizations for $U_\infty = 40\ ms^{-1}$ and $90\ ms^{-1}$ and for angles of attack $\alpha = 0^o, -5^o, -10^o$ and -15^o, which will be mainly related to the computed wall streamlines and the separation patterns.
- Wall pressure measurements (176 pressure taps for a half model) for $U_\infty = 40\ ms^{-1}$ and $90\ ms^{-1}$ and for $\alpha = -15^o$ to 0^o by step of 2.5^o. These results will not be looked in detail here, as they are mainly related to inviscid flow calculations. We will however comment them in relation with the behaviour of the boundary layer calculations.

3 Boundary layer calculations

The method developed at ONERA/CERT/DERAT /Ref. 2, 3/ deals with three–dimensional boundary layer integral equations written in a general surface coordinate system. Starting from given initial conditions (generally provided by stagnation point solutions) and knowing the metrics of the coordinate system (obtained by geometric transformations), integration of the equations proceeds by X-marching and needs the data of boundary conditions.

These conditions consist in magnitude and direction of inviscid velocity at the edge of the boundary layer. In first order theory, this can be achieved using wall

pressure either measured or computed through inviscid flow calculations.

As wall pressure measurements are generally too spaced to provide precisely the magnitude of pressure gradients, the theoretical inviscid velocity at wall is most of the time used. When no large separation exists, this procedure gives good results, a weak interaction iteration being generally enough to ensure correct prediction of the flow. When large separation regions are present, strong interaction should be taken into account in the determination of the pressure field.

In the present paper, calculations have only been done with the inviscid velocity fields computed without the wake /Ref. 4/. As in the first half of the body, agreement between measured and computed wall pressure is good (see example on Fig. 3), we can expect a satisfactory behaviour of boundary layer calculations in this region. When approaching separated region, at the rear of the body, discrepancies arise (Fig. 3) and boundary layer calculations can lead to erroneous results.
All calculations have been performed for $U_\infty = 40\ ms^{-1}$.

4 Results for $\alpha = 0°$

An important preliminary comment is that for all test conditions, oil flow visualizations show the presence of a laminar separation bubble at the beginning of the constant section part of the body (Fig. 6, 13 and 17). If this bubble causes a natural transition (checked by transition visualizations), it is however very large.

We have plotted, on figure 4, the evolution in the transverse direction, of skin friction coefficient and streamwise displacement thickness at station $X = 400\ mm$ located about 280 mm downstream of the bubble. A first calculation assuming bubble giving a transition at separation with continuity on momentum thickness (solid lines) shows a large underestimation of boundary layer thickness. Previous studies /Ref. 5/ have shown that, in two-dimensional flows, separation bubble induces an increase in momentum thickness. The problem here is that this overthickening is not constant around the body, but presents maxima on the centerlines of each flat side of the body ($\varphi = 0$, 90 and 180°). This is due to the strong convergence of the flow induced by three-dimensional effects of the bubble at the longitudinal rounded edges of the body, clearly visible on water tunnel visualizations /Ref. 6/.

Attempts to locally use two-dimensional calculation methods /Ref. 5/ consequently failed. On the other hand, experimental data are too scarce and they cannot be used as initial conditions. We finally had to estimate the overthickening of the bubble all around the body in order to have reasonable agreement at the first measuring station. This was of course only possible for $\alpha = 0$ and $-\ 5°$ when boundary layer measurements were available.

This step being done, calculation can be performed on all the body. Figure 5 presents the corresponding results on the lateral mid line ($\varphi = 90°$) compared with the experimental results. Agreement is quite satisfactory, except in the vicinity of separation, where the evolutions are very steep. If we look on figure 6 the comparison between oil flow visualizations and computed wall streamlines, we find again a very good agreement, except in the vicinity of separation at the rear of the body. Visualizations show a separation line due to an upward accumulation of wall streamlines,

while calculation predicts a too late separation, with a downward behaviour of wall streamlines.

If we examine, on figure 7, the evolution, in the transverse direction, of measured and computed wall pressure distributions, in a section located in this area, we can note, on the side of the model, opposite signs for the transverse pressure gradients leading to opposite curvatures of experimental and computed wall streamlines.

To try to find some explanation, we can look on figures 8 and 9, at contours of longitudinal mean velocity and turbulent kinetic energy measured in the wake, in a plane normal to the longitudinal body axis. If we remind visualizations on figure 6, we can assume, in the lower part of the wake, a behaviour similar to an axisymmetric blunt body separation. If we look then at figure 10, where secondary velocity vectors, in a plane normal to body axis, have been plotted, we can see two small counter rotating vortices, aligned below the tail boom.

In these conditions, influence of the wake on the pressure field at the rear of the body is large; this could explain that inviscid flow calculations without the wake fails to represent accurately the pressure gradients in this area.

5 Results for $\alpha = -5^o$

Figure 11 shows the evolution in the transverse direction at $X = 400\ mm$ of streamwise displacement thickness, measured and computed with estimation of the effect of the bubble. Problems encountered at $\alpha = 0^o$ are here amplified by the dissymmetry due to incidence.

Figure 12 gives the evolutions of streamwise momentum thickness along two characteristic lines ($\varphi = 180^o$: lower symmetry line ; $\varphi = 90^o$: lateral mid line). Calculation without bubble effects has also been plotted (solid line) for $\varphi = 180^o$ to show the importance of it. Comparisons with calculation taking into account bubble effects (dotted line) shows, on this line, a good agreement, up to the locally two-dimensional separation (see Fig. 14). On the side line, as for $\alpha = 0^o$, discrepancies arise when approaching three-dimensional separation.

On figure 13 are compared oil flow visualizations and computed wall streamlines. Agreement is good, except in the vicinity of separation, on the lateral face of the rear part of the body. In particular, calculation is not able to predict the formation of the strong vortex at the rear of the body. This vortex is clearly visible on figure 14 showing rear side view of the oil flow pattern. We can see the locally two-dimensional separation on the lower symmetry line, and the formation of the vortex by accumulation of wall streamlines on both sides of the rounded edge of the body.

The trace of this vortex can also be found on figure 15 and 16, showing secondary velocity plots, in the wake, in two planes normal to body axis. This vortex seems to keep very strong, aligned along the lower side of the tail boom, with a small core of high turbulent kinetic energy.

This change in the wake pattern between 0 and $-\ 5^o$ should be very important to predict, as it is associated with a large increase in drag /Ref. 7/. This is

obviously due to an increase in vortical drag, as can be seen when comparing figures 11 and 15.

6 Results for $\alpha = -10^o$ and -15^o

For these incidences, only pressure measurements and oil flow visualizations were available. However, boundary layer calculations have been performed, from which we have deduced the wall streamlines to be compared with oil flow visualizations. Figure 17 gives an example of these results, for $\alpha = -15^o$.

As for lower incidences, agreement is good on the major part of the body. But, surprisingly, agreement remains good up to separation, the pattern of which being quite well predicted, although the inviscid flow calculation does not take the wake into account.

In fact, up to separation, comparisons between measured and computed pressure fields show better agreement that for lower negative incidences, probably because interaction between the tail boom and the vortical wake is weaker, due to the higher negative incidence. On the side of the rear part of the body, streamlines arrive nearly perpendicular to the rounded edge of the body and separation is much closer to a two-dimensional one, which is easier to predict than a three-dimensionnal one. This is clearly visible on figure 18, showing rear side view of the visualizations, where wall streamlines go nearly straight up to the separation line originated at the lower part of the body.

7 Conclusions

The study of the flow around a simplified helicopter fuselage has been carried out, as part of cooperation between AEROSPATIALE (Helicopter Division) and ONERA.

First part of contribution from DERAT consisted in a detailed study of the model, in the F2 wind tunnel. Pressure measurements, visualizations and mainly three-dimensional LDV surveys provided a large amount of data. This allowed us first a better understanding of the physics of the flow, in particular at the rear part of the body.

On the other hand, comparisons with boundary layer calculations showed that simple inviscid flow calculations could provide boundary conditions giving reasonable overall agreement.

However, a better prediction of aerodynamic characteristics (mainly drag), seems more difficult and should probably go through improvements in the modelling of the wake in inviscid flow calculation.

We can hope this test case will help to develop such procedures.

References

[1] D Afchain, P Broussaud, M Frugier, G Rancarani: *"La soufflerie F2 du centre du Fauga-Mauzac"* presented at 20th AAAF meeting, november 1983.

[2] J Cousteix: *"Analyse theorique et moyen de prevision de la couche limite turbulente tridimensionnelle"* ESA translation TT 238

[3] J Cousteix, C Gleyzes, B Aupoix: *"Analysis of three-dimensional separation by using a boundary layer approach"* Int. Conf. on Fluid Mechanics, Beijing (China), july 1987.

[4] S R Ahmed, J Amtsberg, A De Bruin, A Cler, G Falempin, T H Le, G Poltz, F T Wilson: *"Comparison with experiments of various computational methods of airflow on three helicopter fuselages"* presented at the XIV European Rotorcraft Forum, Milan, september 1988.

[5] C Gleyzes, J Cousteix, JL Bonnet: *"A calculation method of leading edge separation bubbles"* Numerical and physical aspects of aerodynamic flows ,Springer-Verlag, 1983.

[6] H Werle: *"Ecoulements decolles observes sur un fuselage d'helicoptere nu"* ONERA internal report No 152/1369AN611A.

[7] A Cler: *"Affinement fuselages - partie experimentale"* AEROSPATIALE/DH, STPA/HE fiche 2/48, 1986.

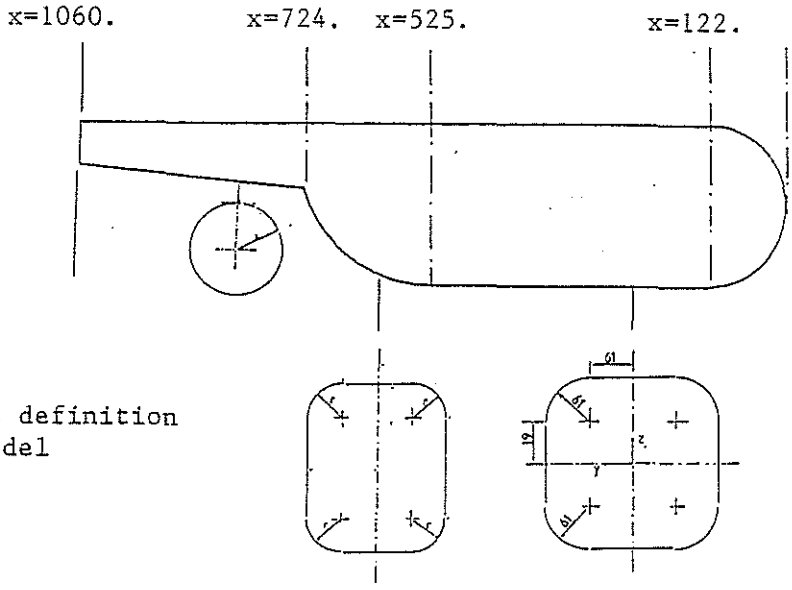

Fig. 1:
Geometric definition
of the model

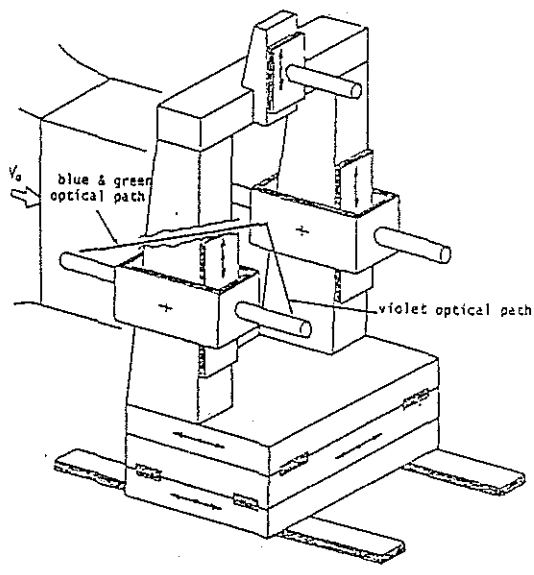

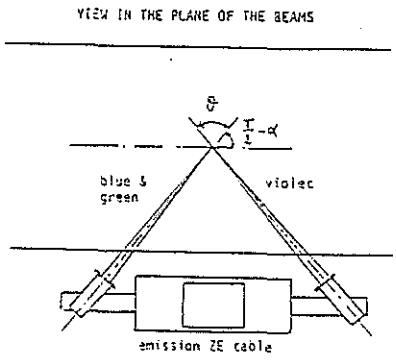

Fig. 2:
3D LDV system

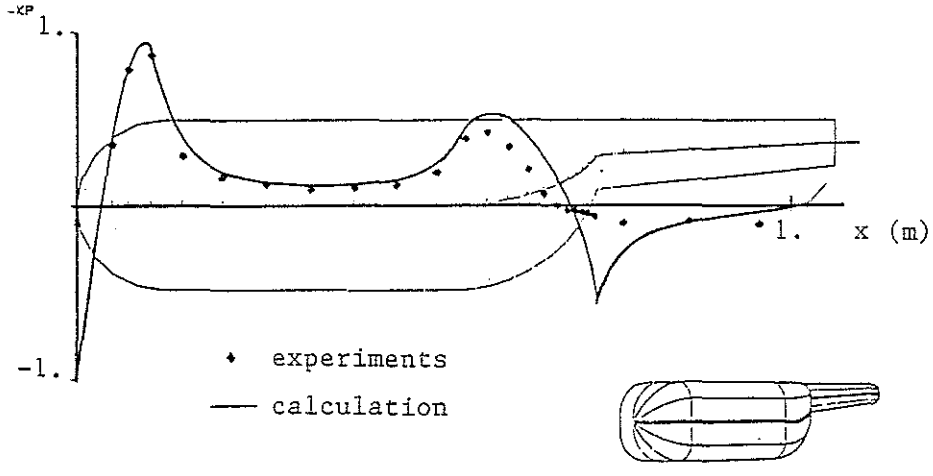

Fig. 3: Pressure distribution along lateral mid-line (α = 0°)

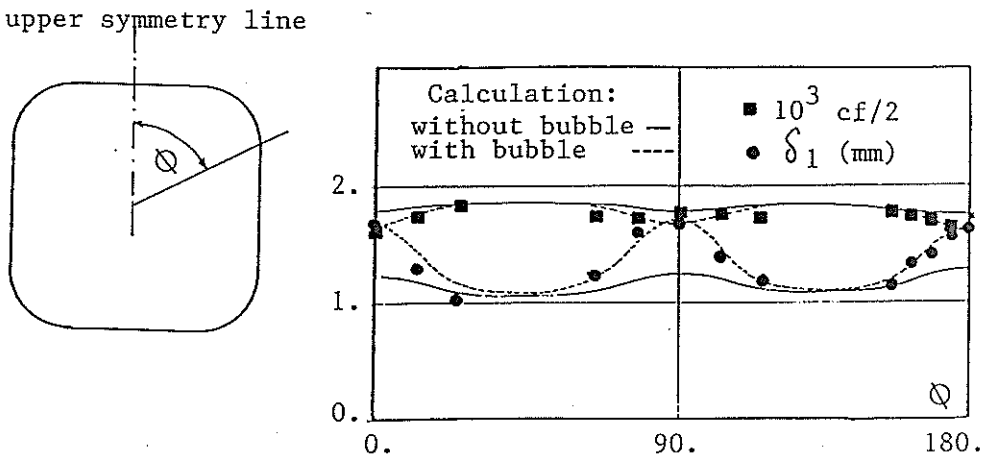

Fig. 4: Evolution of skin friction coefficient and of streamwise displacement thickness in section X=400 mm ; $\alpha = 0°$.

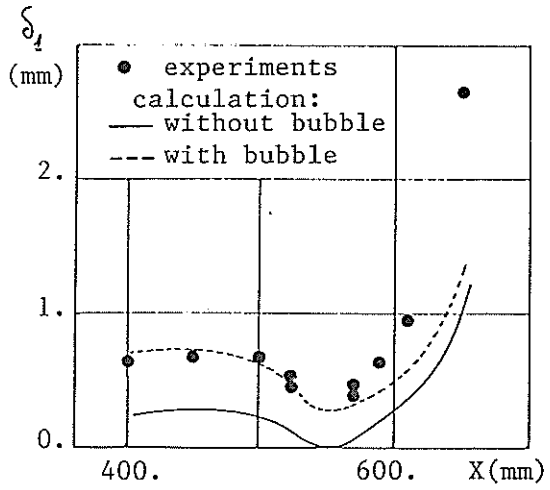

Fig. 5: Evolution of displacement thickness along lateral mid-line

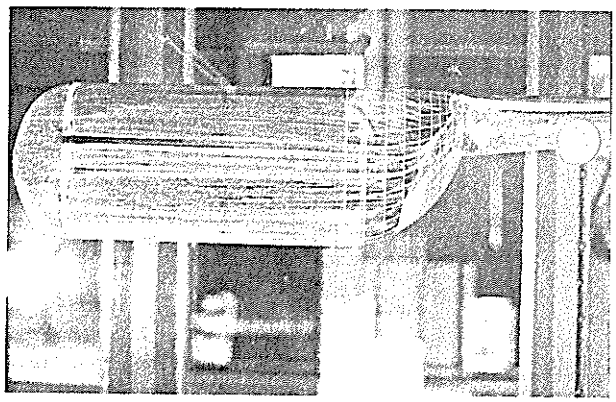

Fig. 6: Comparison of computed and visualized wall streamlines ($\alpha = 0°$)

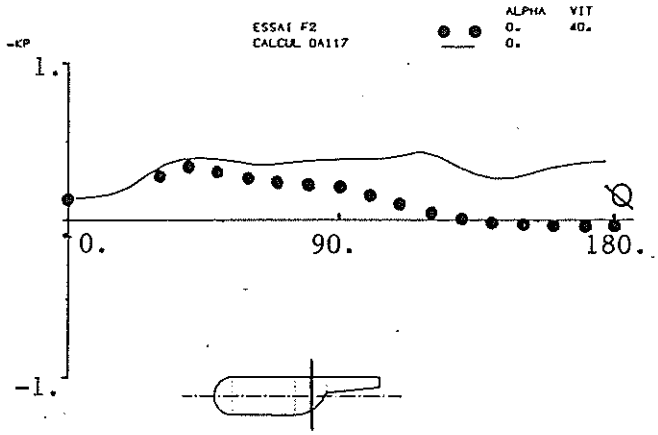

Fig. 7: Crosswise evolution of wall pressure. x=626.5 mm; $\alpha = 0°$

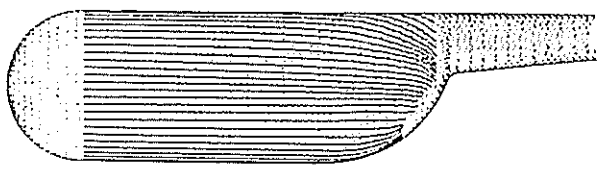

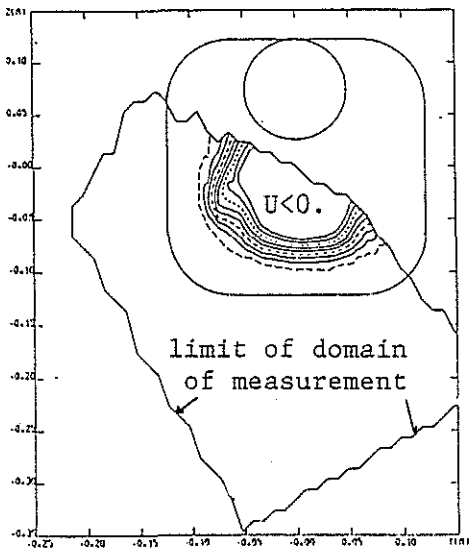

Fig. 8: Contours of longitudinal mean velocity in the wake. (section x=762.5 mm ; $\alpha = 0°$)

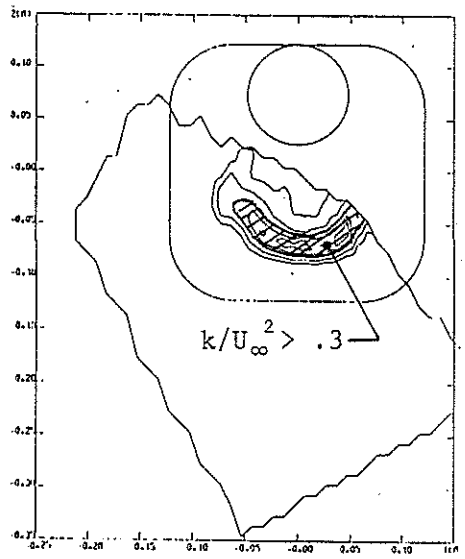

Fig. 9: Contours of turbulent kinetic energy in the wake. (section x=762.5 mm ; $\alpha = 0°$)

Fig. 10: Plot of secondary velocity vectors in a plane normal to body axis (x=762.5mm ; $\alpha = 0°$)

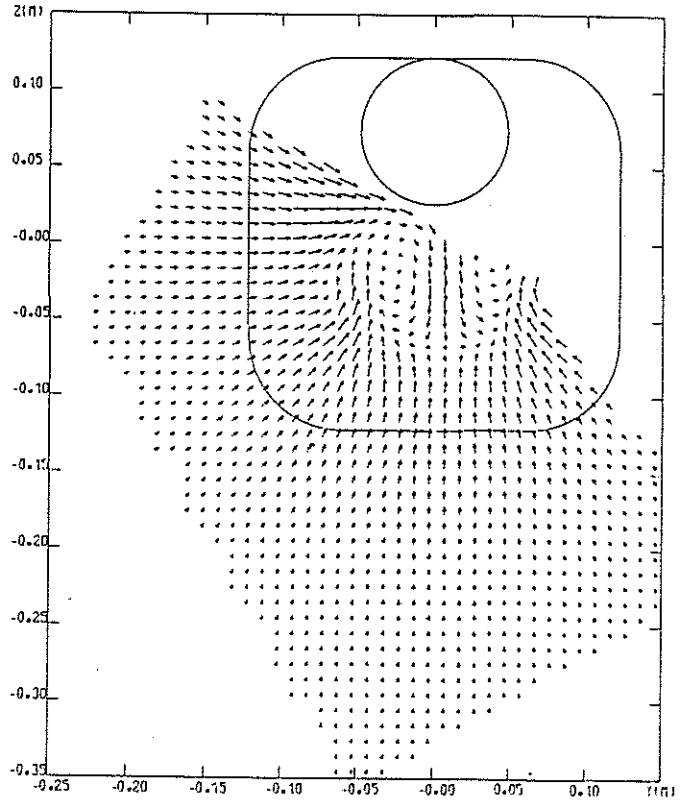

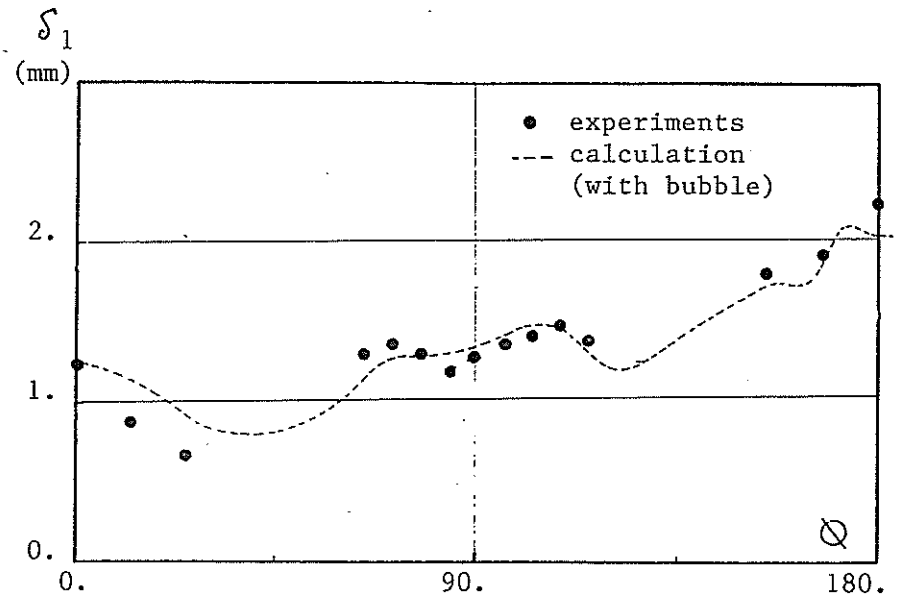

Fig. 11: Evolution of streamwise displacement thickness in section x=400 mm ; α =-5°

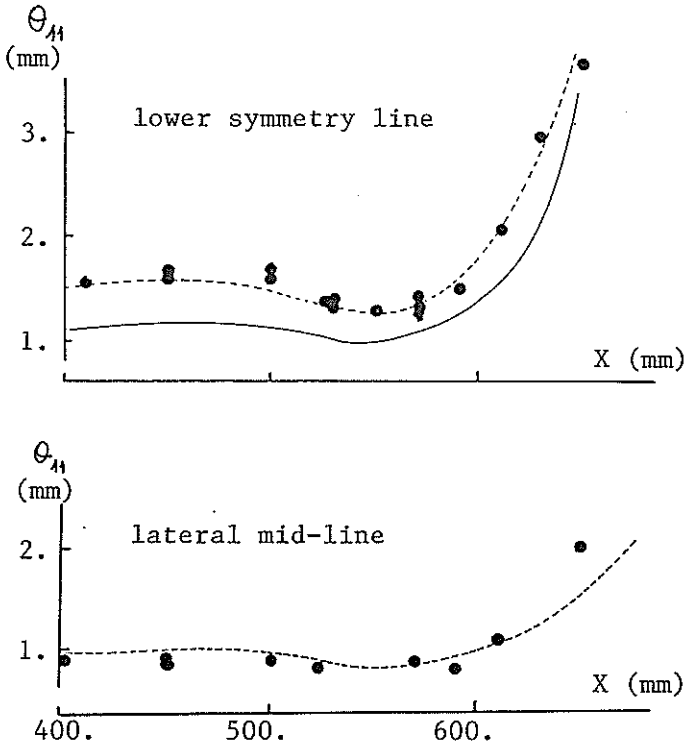

Fig. 12: Evolution of streamwise momentum thickness on two characteristic lines; α =-5°

- experiments
  calculations
  ----- with bubble
  ——— without bubble

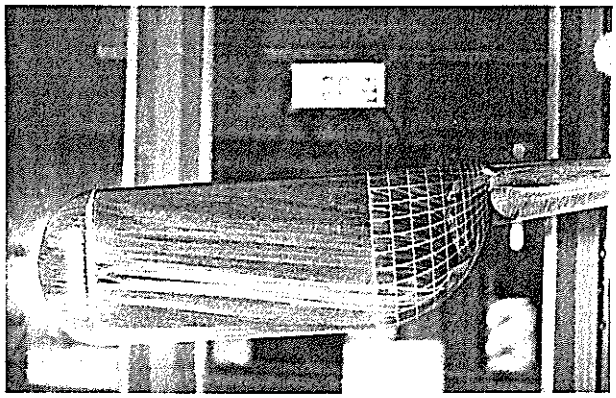

Fig. 13: Comparison of computed and visualized wall streamlines (α =-5°)

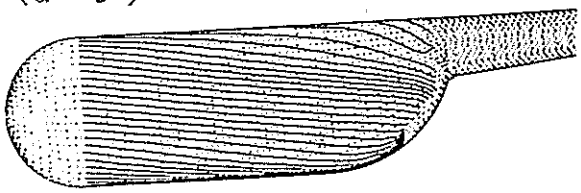

Fig. 14: Rear side view of oil flow visualizations (α=-5°)

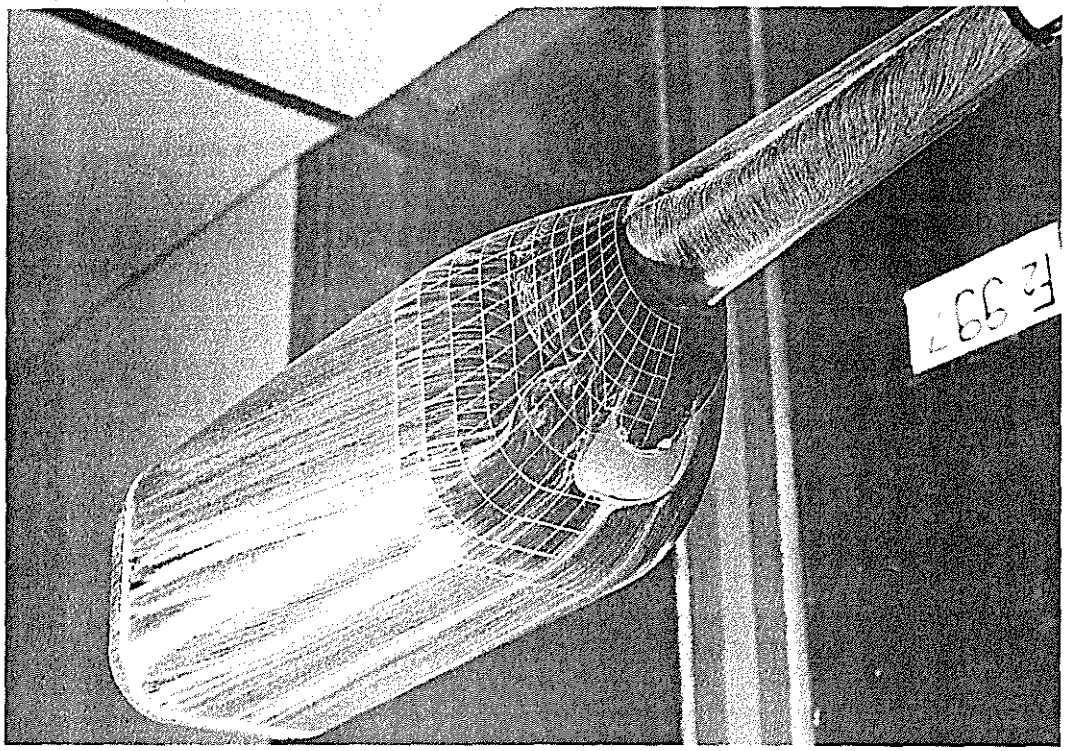

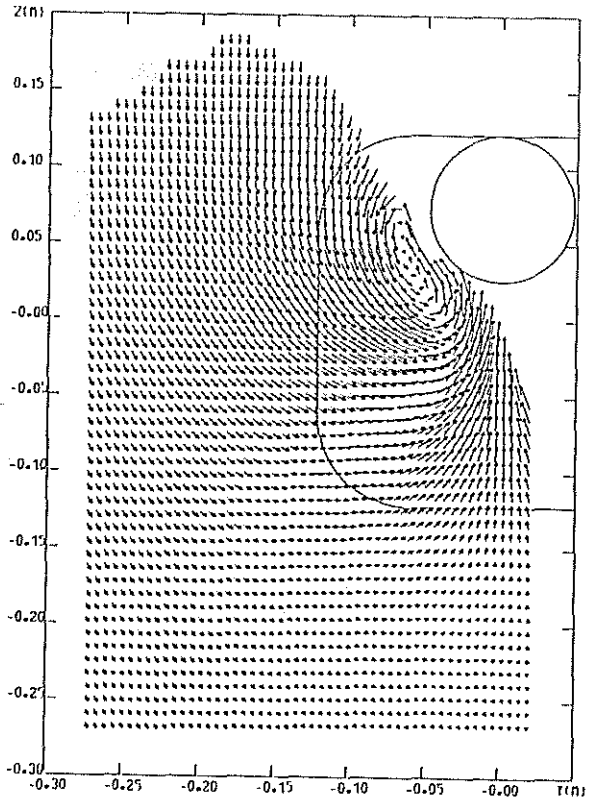

Fig. 15: Secondary velocity vectors in a plane normal to body axis (x=762.5 mm ; α =-5°)

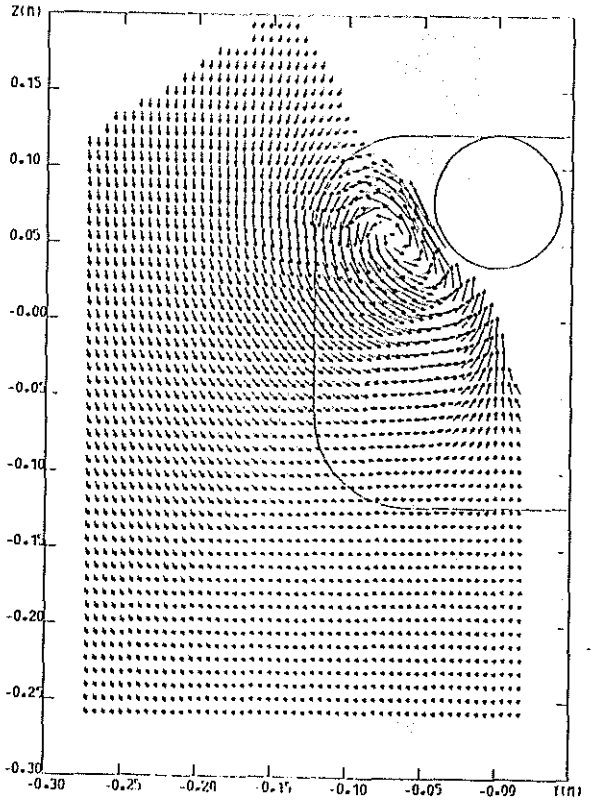

Fig. 16: Secondary velocity vectors in a plane normal to body axis (x=855 mm ; α =-5°)

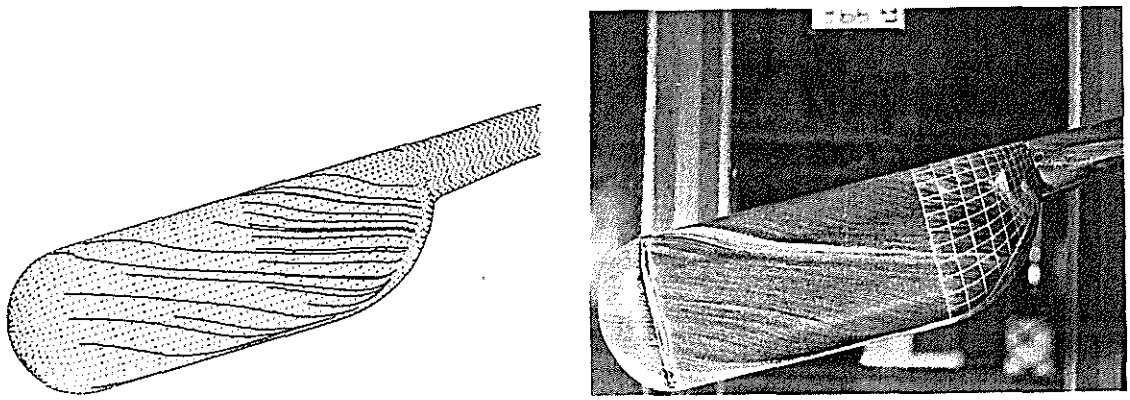

Fig. 17: Comparison of computed and visualized wall streamlines ($\alpha = -15°$)

Fig. 18: Rear side view of oil flow visualizations ($\alpha = -15°$)